PHYSICAL REVIEW E VOLUME 60, NUMBER 4 OCTOBER 1999

Instabilities of cavity solitons in optical parametric oscillators

Dmitry V. Skryabin*
Department of Physics and Applied Physics, University of Strathclyde, Glasgow G4 0NG, Scotland
(Received 20 April 1999)

Using an example of cavity solitons in optical parametric oscillators it is demonstrated that Hopf instability of these dissipative structures can be directly associated with internal modes of their conservative counterparts. The latter ones are free propagating quadratic solitons in this case. Linear stability analysis and numerical simulation also reveal multistability and complex instability induced spatiotemporal dynamics of single and multihump cavity solitons. [S1063-651X(99)51110-0]

PACS number(s): 42.65.Tg, 05.45.Yv

Localized structures (LS) in the nonlinear dissipative systems driven far from an equilibrium attract a great deal of interdisciplinary interest [1–9]. Their stability is still largely open and important for the experimental observations problem. No general criterion has been suggested for the prediction of the instabilities of LS until now and most of the theoretical analyses were restricted by numerical observations of stable and unstable regimes [1–9]. On the other hand, the theory of stability of LS in conservative Hamiltonian systems has been successfully developed over the last three decades; see, e.g., [2,10–13].

Nonlinear optics is one of the fields where a rich variety of LS was found theoretically [2–11] and observed in experiments [14–16]. In particular, parametric wave mixing in media with cubic and quadratic nonlinearities is known to support single or multifrequency solitons; see, e.g., [7–15]. Parametric interaction can be efficiently realized both in free propagation and intracavity schemes. The former were successfully approximated by the energy conserving Hamiltonian [2,10–15] and the latter by the dissipative non-Hamiltonian [2–9,16,17] models. Therefore, one can apply knowledge of the stability and spectral properties of the free propagating ''Hamiltonian'' solitons, in order to understand their modification under the action of dissipation and external driving, relevant in the description of the intracavity processes.

This idea was applied before in different physical contexts using the perturbed one-dimensional (1D) nonlinear Schrödinger (NLS) equation [6]. Instabilities of LS described in [6] appear due to bifurcations involving discrete soliton eigenmodes, which split from the edge of the continuous spectrum under the action of perturbations. The full set of eigenmodes associated with the single-hump solitons in unperturbed 1D NLS equations is known analytically [18]. It consists of the zero-eigenvalue eigenmodes generated by symmetries and unbounded eigenmodes of the continuum. However, it has been recently shown that solitons in a variety of Hamiltonian models possess the so-called *internal modes* [12,13], i.e., stable localized eigenmodes with nonzero eigenvalues. One of the objectives of this work is to reveal *the role played by these modes of the free propagating parametric solitons in the stability and dynamics of the solitons locked inside a cavity*; i.e., cavity solitons (CS).

Recent theoretical advances in the properties of the free propagating solitons due to three-wave mixing in $\chi^{(2)}$ media [11,12] have shown that $\chi^{(2)}$ solitons have the internal modes. As was demonstrated numerically, the externally pumped optical cavities filled with $\chi^{(2)}$ material can also support CS [7–9]. Recent intensive work in the direction to achieve an efficient frequency conversion in semiconductor microcavities [19], the ongoing wave of the experimental results on transverse instabilities [20], and the recent observations of the plane wave bistability [21] in quadratically nonlinear cavities pave the way towards the experimental observation of $\chi^{(2)}$-CS. Therefore, stability of $\chi^{(2)}$-CS becomes an interesting and important problem not only from the fundamental but also practical viewpoints.

It is noteworthy that the soliton instabilities in free propagation schemes are *convective* ones, i.e., perturbations grow with propagation. Therefore, even if a soliton is actually unstable in a particular range of parameters, the stable trapping can still be observed over the short length of a nonlinear sample. To the contrary, in most of the cavity schemes stability and instability are *absolute*, i.e., perturbations grow in time at a fixed spatial point; therefore, unstable CS either disappear or produce other spatiotemporal structures on the time scale of the characteristic cavity photon lifetime. Thus stability of the CS is an essential prerequisite for their experimental observation.

We will concentrate below on CS in optical parametric oscillators (OPO) and start our analysis transforming mean-field equations for OPO [7,8] describing interaction of the phase matched signal and pump envelopes in a dimensionless quasi-Hamiltonian form

$$(\partial_t+\gamma_m)E_m=i\frac{\delta H}{\delta E_m^*},\quad m=1,2, \tag{1}$$

where H is the functional,

$$H=\int dx\Big[-\alpha_1|\partial_x E_1|^2-\alpha_2|\partial_x E_2|^2+\delta_1|E_1|^2+\delta_2|E_2|^2 +\frac{1}{2}(E_1^2E_2^*+\mu E_1^2+\text{c.c.})\Big].$$

*URL:http://enqo.phys.strath.ac.uk~dmitry

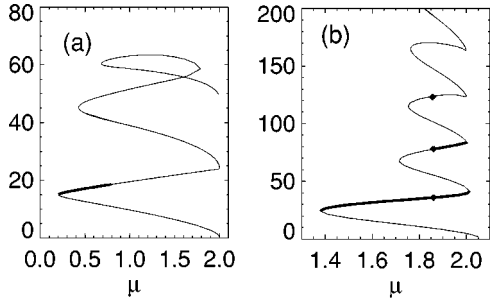

FIG. 1. Energy of the soliton signal field, $Q_1=\int dx|A_1|^2$, vs pump μ. (a) $\gamma_{1,2}=0.1$, $\delta_{1,2}=-2$; (b) $\gamma_1=1$, $\gamma_2=0.8$, $\delta_1=-1.8$, $\delta_2=-4$. Bold and thin lines mark, respectively, stable and unstable solitons.

t is the time measured in the units of $\tau_c s$, where τ_c is the cavity roundtrip time and s is an arbitrary scaling constant. $\gamma_m=T_m s/2$, here T_m are the mirror transmitivities. $x=X[2k_1/(sL)]^{1/2}$ and $\alpha_m=k_1/k_m$, where X is the transverse coordinate in physical units, k_m are the the wave vectors, $2k_1=k_2$, and L is the cavity roundtrip length. $\delta_m=s\tau_c(m\omega-\omega_m^{cav})$ are the detunings from the cavity resonances ω_m^{cav} and ω is the signal frequency. μ is linked with the external pump field E_p via $E_p=\mu\sqrt{2(\delta_2^2+\gamma_2^2)}/(s\tau_c\chi^{(2)}\omega\sqrt{2T_2})$, here $\chi^{(2)}$ is the effective quadratic susceptibility. Expressions for fields in physical units $\mathcal{E}_m$ are given by $\mathcal{E}_1=2E_1e^{i\psi/2}/(s\tau_c\chi^{(2)}\omega)$, $\mathcal{E}_2=\sqrt{2}e^{i\psi}(E_2+\mu\sqrt{\delta_2^2+\gamma_2^2})/(s\tau_c\chi^{(2)}\omega)$, here $\psi=-\arctan(\gamma_2/\delta_2)$. The mean-field model is a robust approximation and is often used to describe cavity dynamics even sufficiently far from the limits of its formal validity, which require detunings and cavity linewidths to be much less than half of the cavity free spectral range, and therefore we will assume below soft conditions $\gamma_m,\delta_m<s\pi$ instead of $\ll$.

Among different bright and dark localized structures found in the numerical modeling of the OPO [7,8] we choose bright CS sitting on a zero background field [7]. A family of multihump CS exists inside the pump range $\mu_L<\mu<\mu_R$ providing that $\delta_m<0$, where $\mu_R=\sqrt{\delta_1^2+\gamma_1^2}$ and $\mu_L=|\gamma_1\delta_2+\gamma_2\delta_1|/\sqrt{\delta_2^2+\gamma_2^2}$. This fact was verified by numerical solution of ordinary differential equations $\gamma_m A_m=i\delta H/\delta A_m^*$, here $A_m(x)=E_m(x,t)$. The conditions imposed on μ and δ_m are in fact conditions for the coexistence of two nontrivial, $A_m\neq 0$, homogeneous, $\partial_x A_m=0$, solutions and a trivial one, $A_m=0$ [21]. Numerically built graphs of the energy of the signal field vs external pump μ for two different parameter sets and typical transverse profiles of the CS are presented, respectively, in Figs. 1 and 2. For μ close to the μ_R upper

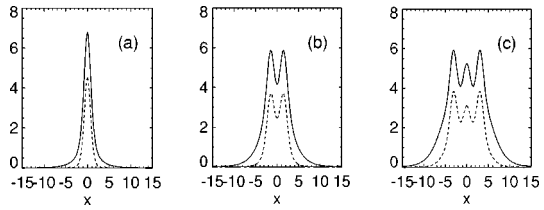

FIG. 2. Transverse profiles of $|A_1|$ (solid lines) and $|A_2|$ (dashed lines) for the single-, two- and three-hump solitons marked by the rhombs in Fig. 1(b).

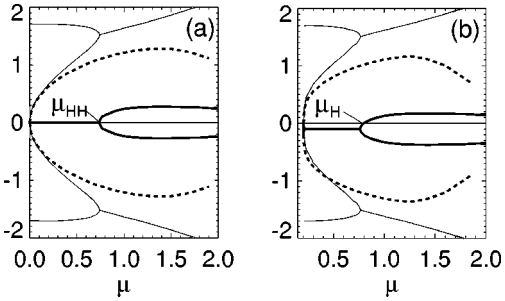

FIG. 3. Real (bold solid and dashed lines) and imaginary (thin solid lines) parts of the eigenvalues governing stability of the upper (bold and thin solid lines) and low (dashed lines) branches of the single-hump solitons vs pump μ for $\delta_{1,2}=-2$. (a) $\gamma_{1,2}=0$, (b) $\gamma_{1,2}=0.1$.

branch of the single-hump CS, i.e., the branch with larger energy, bifurcates back into a sequence of the higher order multihump CS. While existence of the single- and two-hump solitons was numerically demonstrated before [7], their link with each other and with the higher-order solitons is a novel feature.

After the brief summary of the existence problem is given we turn our attention to the main problem we want to address here, i.e., to the stability of CS with respect to small perturbations. We seek solutions of Eqs. (1) in the form $A_m(x)+\varepsilon[U_m(x,t)+iW_m(x,t)]$, where $\varepsilon\ll 1$. After the standard linearization and substitutions $U_m=u_m(x)e^{\lambda t}$, $W_m=w_m(x)e^{\lambda t}$ we derive an eigenvalue problem $\lambda\vec{\xi}=\hat{\mathcal{L}}\vec{\xi}$, where $\vec{\xi}=(w_1,w_2,u_1,u_2)^T$ and $\hat{\mathcal{L}}$ is the linearization of Eqs. (1) near a soliton. The discrete spectrum of the non-self-adjoint differential operator $\hat{\mathcal{L}}$ has been found numerically using second-order finite differences.

Let us start the discussion of the stability properties focusing on the single-hump CS. To understand the origin of their instability it is convenient to consider a limit situation when Eqs. (1) become Hamiltonian, i.e., $\gamma_m\to 0$. It appears that CS do exist in this limit. However, they are still very different from $\chi^{(2)}$ solitons in the free propagation geometry [11]. One of the reasons for this is that the total energy $\int dx(|E_1|^2+2|E_2|^2)$ is not a conserved quantity in our case. It becomes conserved and CS become equivalent to the free propagating solitons only when pump photons are not injected into a cavity any more, i.e., $\mu=0$. Then, in accord with Noether's theorem, Eqs. (1) acquire the phase symmetry, $E_m\to E_m e^{im\phi}$, which in turn generates eigenmode $\vec{\xi}_0=(\mathrm{Re}A_1, 2\mathrm{Re}A_2, -\mathrm{Im}A_1, -2\ \mathrm{Im}A_2)^T$ with double zero eigenvalues, $\hat{\mathcal{L}}\vec{\xi}_0=0$. For $\gamma_m=0$ the left existence boundary of the CS is $\mu=\mu_L=0$. Let us first deviate μ from zero moving along the low branch of the single-hump solitons, i.e., the branch with smaller signal energy; see Fig. 1. In this case the two zero eigenvalues associated with $\vec{\xi}_0$ split and move along the real axis, $\mathrm{Im}\lambda=0$, of the (Reλ,Imλ) plane in the opposite directions; see the dashed lines in Fig. 3(a). Thus, the low soliton branch is unstable due to the presence of the positive eigenvalue in the soliton spectrum. On the contrary, moving along the upper soliton branch we have found that the zero eigenvalues move in the opposite directions along the imaginary axis, $\mathrm{Re}\lambda=0$; see the thin solid lines in Fig. 3(a). Thus, the upper soliton branch remains

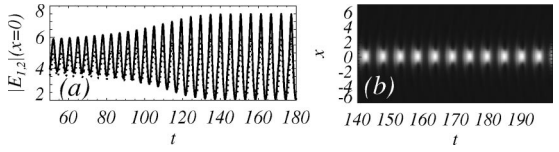

FIG. 4. Stable pulsations of the upper-branch single-hump soliton in the region of its Hopf instability. Full and dotted lines in (a) mark, respectively, $E_1(t)$ and $E_2(t)$ at $x=0$. (b) shows $|E_1(x,t)|$ [22]. $\mu=0.8$ and other parameters as in Fig. 1(a).

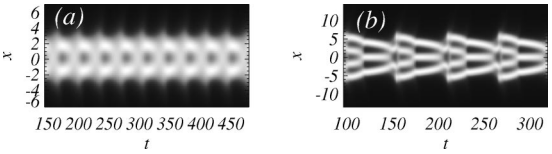

FIG. 5. Spatiotemporal evolution of $|E_1|$ [22] resulting from Hopf instability of two-hump (a) and four-hump (b) solitons. (a) $\mu=1.8$, (b) $\mu=1.9$. Other parameters as in Fig. 1(b).

stable at least for small μ. However, at some $\mu=\mu_{HH}$ these eigenvalues meet a pair of other purely imaginary eigenvalues which are the direct continuation of the eigenvalues corresponding to the *internal* eigenmodes of the free propagating quadratic solitons [12]. This collision leads to the onset of the Hamiltonian-Hopf instability of the CS; see the bold solid lines in Fig. 3(a).

Introducing linear losses, which are unavoidable in a real cavity, and keeping them equal for the both harmonics one will find that the bifurcation diagram simply shifts down along the axis $\mathrm{Im}\lambda=0$ by the value equal to γ_m; see Fig. 3(b). Non-Hamiltonian corrections transform the Hamiltonian-Hopf bifurcation into the standard Hopf bifurcation ($\mu_{HH}\rightarrow\mu_H$) [see Fig. 3(b)] well known for the dissipative systems [1]. It follows, see Fig. 3, that the higher the losses are, the higher the pump power needed to approach the Hopf instability threshold. Assuming that $s=1$ Figs. 1(a) and 3(b) correspond to the physical situation with large detunings and 10% losses.

It is interesting to check how stability properties of the CS vary when the cavity is tuned closer to resonances at both frequencies. CS become wider near the resonances, and to avoid large computational windows we take advantage of using different scaling and fix $s=2/T_\omega$. Thus, $\gamma_m\sim 1$ physically corresponds to the same 10% losses, but $\delta_m\sim 1$ corresponds now to detunings of the order 0.1 of the free spectral range. One can see from Fig. 1(b) that small detunings and/or large losses have stabilizing effects and the coexistence of the stable single- and two-hump CS is possible.

Note that the Hopf instability found here cannot be interpreted as due to the known Hopf instability of the upper branch of the homogeneous solution [17], because the latter one is Hopf unstable only for $\delta_1\delta_2<0$, where the considered CS family does not exist. Thus, all the dynamics described here are direct consequences of the transverse localization. Proto-Hopf eigenmodes of the soliton exist in a wide range of parameters in the CS stability region and a simple experimental method of their detection can be suggested. The weak probe beam localized in the soliton region and passing through the cavity mirrors without significant reflection should be resonantly absorbed in the cavity providing that the beam frequency coincides with $\mathrm{Im}\lambda$ of the proto-Hopf eigenmode.

To study the dynamics of the Hopf unstable CS an extensive series of the numerical simulations has been performed. Inside the instability region, but close to the critical boundary, a stable attractor in the form of an oscillating CS has been found; see Fig. 4 [22]. Deeper inside the instability region we have observed two scenarios of the soliton destruction. For some intermediate region of μ the growing amplitude of the oscillations leads to the switching into the trivial solution. Then for μ close enough to μ_R the pulsating soliton easily excites chaotic pattern, which quickly fills the entire computational window. A possible interpretation of the last scenario is that the radiation escaping from the oscillating soliton along its tails (which are weakly damped when μ is close to μ_R) locally produces parametric gain sufficient to excite a chaotic pattern existing near the upper branch of the homogeneous solution.

Two spatially localized periodic attractors have been found taking the multihump CS as an initial condition. One of them corresponds to the Hopf unstable two-hump CS [see Fig. 5(a)], and another one to the Hopf-unstable three- or four-hump CS [see Fig. 5(b)]. The dynamical regimes shown in Figs. 4 and 5 also serve as attractors for a wide range of experimentally relevant initial conditions in a form of Gaussian pulses of the pump radiation with suitable width, height, and duration.

Let us take a 1 cm long monolithic planar waveguide cavity with $\chi^{(2)}\simeq 20$ pm/V, which is typical, e.g., for a noncritically phase matched potassium niobate crystal, with an elliptical pump beam at frequency $\sim 10^{15}$ Hz focused into the $\sim$1mm wide and $\sim 1\mu$m thick waveguide. These parameters give estimation of the real world pump power $\sim\mu^2(\delta_2^2+\gamma_2^2)/s^2\times 10$ W, of the cavity soliton size $\sim\sqrt{s10^3}$ μm and of the typical frequency of the Hopf oscillations $\sim(10^9/\mathrm{s})$Hz.

Considering an extension of our results to other externally driven nonlinear optical cavities and generally to other dissipative systems we have to say that if in the absence of the external driving and losses a model has solitary solutions then one can expect similar bifurcation scenarios. The reasons for this are that an external pump always breaks the phase symmetry associated with the energy conservation and losses destroy the Hamiltonian structure in a manner similar to that described in the present context. However, this symmetry breaking is sufficient only for an appearance of the stable upper and unstable low CS branches, but it is not sufficient for the Hopf instability of the upper branch. Another important ingredient, which ensured this instability in the case of CS in OPO, is the presence of the *internal* soliton modes in the limit when the pump and losses are negligible. These modes have already been demonstrated in several models describing free propagating optical solitons, see, e.g., [12,13], and admitting their cavity generalizations.

In summary, stability, multistability, and instability of the single and multihump cavity solitons in the degenerate optical parametric oscillators have been examined by means of the linear stability analysis and numerical simulation of the dynamical and stationary equations. It is demonstrated that

Hopf instability leading to complex spatially localized dynamics originates from the presence of the internal modes of the free propagating quadratic solitons.

The author thanks A.R. Champneys, C. Etrich, W.J. Firth, and G.-L. Oppo for stimulating discussions of relevant questions. He also acknowledges financial support from the Royal Society of Edinburgh and British Petroleum. The work is partially supported by ESPRIT project PIANOS and EPSRC Grant No. GR/M19727.

[1] M.C. Cross and P.C. Hohenberg, Rev. Mod. Phys. **65**, 851 (1993).

[2] N.N. Akhmediev and A. Ankievich, *Solitons: Nonlinear Pulses and Beams* (Chapman & Hall, London, 1997).

[3] P. Mandel, *Theoretical Problems in Cavity Nonlinear Optics* (Cambridge University Press, Cambridge, England, 1997).

[4] N.N. Rosanov, Prog. Opt. **35**, 1 (1996); W.J. Firth and A.J. Scroggie, Phys. Rev. Lett. **76**, 1623 (1996); M. Brambilla *et al.*, *ibid.* **79**, 2042 (1997).

[5] R.J. Deissler and H.R. Brand, Phys. Rev. Lett. **72**, 478 (1994); V.V. Afanasjev, N. Akhmediev, and J.M. Soto-Crespo, Phys. Rev. E **53**, 1931 (1996); X. Wang and R. Wei, Phys. Rev. Lett. **78**, 2744 (1997); D. Michaelis, U. Peschel, and F. Lederer, Opt. Lett. **23**, 1814 (1998).

[6] K. Nozaki and N. Bekki, Physica D **21**, 381 (1986); M. Bondila, I.V. Barashenkov, and M.M. Bogdan, Physica D **87**, 314 (1995); T. Kapitula and B. Sandstede, J. Opt. Soc. Am. B **15**, 2757 (1998); N.V. Alexeeva, I.V. Barashenkov, and D.E. Pelinovsky, Nonlinearity **12**, 103 (1999).

[7] K. Staliunas and V.J. Sánchez-Morcillo, Opt. Commun. **139**, 306 (1997); S. Longhi, Phys. Scr. **56**, 611 (1997); S. Trillo and M. Haelterman, Opt. Lett. **23**, 1514 (1998); D. V. Skryabin and W. J. Firth, *ibid.* **24**, 1056 (1999).

[8] M. Tlidi, P. Mandel, and M. Haelterman, Phys. Rev. E **56**, 6524 (1997); M. Tlidi, P. Mandel, and R. Lefever, Phys. Rev. Lett. **81**, 979 (1998); K. Staliunas, *ibid.* **81**, 81 (1998); G.L. Oppo, A.J. Scroggie, and W.J. Firth, J. Opt. Soc. Am. B **1**, 133 (1999); M. Le Berre *et al.*, *ibid.* **1**, 153 (1999).

[9] C. Etrich, U. Peschel, and F. Lederer, Phys. Rev. Lett. **79**, 2454 (1997).

[10] E. Kuznetsov, A. Rubenchik, and V. Zakharov, Phys. Rep. **142**, 103 (1986); V.G. Makhankov, Y.P. Rybakov, and V.I. Sanyuk, Usp. Fiz. Nauk **164**, 121 (1994) [Phys. Usp. **37**, 113 (1994)].

[11] D.E. Pelinovsky, A.V. Buryak, and Y.S. Kivshar, Phys. Rev. Lett. **75**, 591 (1995); D.V. Skryabin and W.J. Firth, *ibid.* **81**, 3379 (1998).

[12] C. Etrich *et al.*, Phys. Rev. E **54**, 4321 (1996).

[13] D.E. Pelinovsky, V.V. Afanasjev, and Y.S. Kivshar, Physica D **116**, 121 (1998); Y.S. Kivshar *et al.*, Phys. Rev. Lett. **80**, 5032 (1998); B.A. Malomed and R.S. Tasgal, Phys. Rev. E **58**, 2564 (1998).

[14] J.U. Kang *et al.*, Phys. Rev. Lett. **76**, 3699 (1996).

[15] W.E. Torruellas *et al.*, Phys. Rev. Lett. **74**, 5036 (1995).

[16] M. Saffman, D. Montgomery, and D.Z. Anderson, Opt. Lett. **19**, 518 (1994); V.B. Taranenko, K. Staliunas, and C. Weiss, Phys. Rev. Lett. **81**, 2236 (1998); K. Staliunas *et al.*, Phys. Rev. A **57**, 599 (1998).

[17] L.A. Lugiato *et al.*, Nuovo Cimento A **10**, 959 (1988).

[18] D. Kaup, Phys. Rev. A **42**, 5689 (1990).

[19] V. Berger, in *Advanced Photonics with Second-order Optically Nonlinear Processes*, edited by A. D. Boardman *et al.* (Kluwer, Dordrecht, 1998), pp. 345–374.

[20] V. Sirutkaitis *et al.*, J. Opt. Soc. Am. B **1**, 139 (1999).

[21] C. Richy *et al.*, J. Opt. Soc. Am. B **12**, 456 (1995); A.G. White, J. Mlynek, and S. Schiller, Europhys. Lett. **35**, 425 (1996).

[22] Only the central third of the computational window along x is shown in Figs. 4(b) and 5.